Freak waves and electrostatic wavepacket modulation in a quantum electron–positron–ion plasma

2014 Plasma Phys. Control. Fusion 56 035007

(http://iopscience.iop.org/0741-3335/56/3/035007)

IOP Publishing Plasma Physics and Controlled Fusion

Plasma Phys. Control. Fusion **56** (2014) 035007 (17pp) doi:10.1088/0741-3335/56/3/035007

Freak waves and electrostatic wavepacket modulation in a quantum electron–positron–ion plasma

M McKerr[1], I Kourakis[1] and F Haas[2]

[1] Centre for Plasma Physics, School of Mathematics and Physics, Queen's University Belfast, BT7 1NN Belfast, Northern Ireland, UK
[2] Departamento de Física, Universidade Federal do Paraná, 81531-990, Curitiba, Paraná, Brazil

Received 2 July 2013, revised 8 January 2014
Accepted for publication 13 January 2014
Published 5 February 2014

Abstract

The occurrence of rogue waves (freak waves) associated with electrostatic wavepacket propagation in a quantum electron–positron–ion plasma is investigated from first principles. Electrons and positrons follow a Fermi–Dirac distribution, while the ions are subject to a quantum (Fermi) pressure. A fluid model is proposed and analyzed via a multiscale technique. The evolution of the wave envelope is shown to be described by a nonlinear Schrödinger equation (NLSE). Criteria for modulational instability are obtained in terms of the intrinsic plasma parameters. Analytical solutions of the NLSE in the form of envelope solitons (of the bright or dark type) and localized breathers are reviewed. The characteristics of exact solutions in the form of the Peregrine soliton, the Akhmediev breather and the Kuznetsov–Ma breather are proposed as candidate functions for rogue waves (freak waves) within the model. The characteristics of the latter and their dependence on relevant parameters (positron concentration and temperature) are investigated.

Keywords: electrostatic waves, rogue waves, freak waves, nonlinear Schrödinger equation, quantum plasmas, degenerate plasmas, Fermi plasmas

(Some figures may appear in colour only in the online journal)

1. Introduction

Large ensembles of charged particles (plasmas) have tacitly been used as testbed for nonlinear theories. Many successful models have been proposed for classical plasma description. Whether the many-particle system is modeled as a mixture of charged fluids, or via a kinetic approach, a large number of observable plasma phenomena can be explained from basic physical assumptions.

The classical plasma description bears its own limitations, however. From a fundamental point of view, when densities are large and/or temperatures are low, new effects come into play whose description lies beyond the boundaries of classical mechanics. A high density requires a short inter-particle distance, which in turn results in a nonnegligible overlap among particle wavefunctions. A pressure effect thus arises due to Pauli's exclusion principle, which resists the compression of the particles [1–3].

The study of quantum plasmas has received considerable impetus since the introduction of the multifluid quantum plasma model [4]. Electrostatic modes are of relevance in semiconductor physics where the small dynamical scales require the inclusion of quantum effects such as tunneling [5], and also at the opposite end of the scale in astrophysical plasmas [6].

Various aspects of linear [1, 7–9] and nonlinear [5–14] electrostatic wave propagation have so far been investigated, mainly involving the quantum effect due to electron pressure on the ion dynamics [5–13], but also charged dust concentration effects [8] and modified electron dynamical effects [14]. Different nonlinear paradigms have been employed in the description of quantum plasmas. A Korteweg–de Vries (KdV) equation was derived for ion-acoustic solitary waves in a cold quantum dusty plasma in [8], later extended to a two-dimensional Zakharov–Kuznetsov related description [11]. A modified KdV equation was derived in [12] to describe the evolution of kink-type structures in unmagnetized electron–positron–ion plasmas. That work was later extended to a two-dimensional geometry [10] based on a Kadomtsev–Petviashvili type description or, alternatively, for dense

magnetized plasmas, a Zakharov–Kuznetsov model [9]. In all of these works, ions were treated as classical particles, while quantum effects were introduced via the electron statistics.

One of many generic nonlinear mechanisms dominating wavepacket propagation in plasmas is amplitude modulation, accounting for a variation of the wavepacket's amplitude, resulting in a nonlinear frequency shift [15, 16]. In general, this is described by a nonlinear Schrödinger equation (NLSE) [17], which can be obtained from the plasma-fluid dynamical equations via a multiscale technique [15, 16]. Such a viewpoint was adopted in [13] for ion-acoustic wavepackets in a dense electron–ion quantum plasma, followed by a similar study on electron-scale wavepackets [14], incorporating diffraction effects from the so-called Bohm potential. Modulated wavepackets may be unstable to small perturbations, due to external noise (plasma turbulence). This modulational instability mechanism is not only well known to dominate, e.g., transmission of information along optical fibers, but is also of importance in other fields of physics [18]. Although the modulational mechanism is only tractable analytically in a weak-amplitude regime, it has been postulated as an intermediate stage toward a fully developed instability, which may lead to the formation of envelope pulses, e.g. in nonlinear materials [19], but also in plasmas [20]. An unstable solution subject to modulational instability may exhibit exponential growth or decay. Interestingly, it has recently been suggested that this physical mechanism might underlie the generation of rogue waves (freak waves) in the ocean [21].

In the quantum plasma framework, one can compare the effects due to Fermi statistics and quantum diffraction by means of a nondimensional quantity given by the ratio between the Fermi energy and the plasmon energy of the charge carriers [22]. Typically, for ultra-small semiconductor devices the quantum diffraction represented by the Bohm potential term becomes dominant. However, for highly degenerate dense plasmas obtained in laser compression schemes or astrophysical settings like white dwarfs and neutron stars one can safely neglect the Bohm term.

Recently, a lot of attention has been paid to the physics of electron–positron–ion quantum plasmas. In [23], the ion-acoustic soliton formation in relativistic degenerate electron–positron–ion (e–p–i) plasma was investigated, with higher order nonlinear effects taken into account in [24]. A fully relativistic equation of state was assumed in [25]. In [26], the nonlinear dynamics of dusty electron–positron–ion plasma was studied, assuming traveling wave solutions.

Modulational instability as an efficient mechanism for energy localization has been associated with the occurrence of so-called rogue waves (or freak waves) in the open sea [27, 28]. Such ultra-high *ghost waves* are reported to occur unexpectedly, propagate for short times and then disappears without a trace [29, 30]. Rogue waves (or freak waves, or monster waves, or rogons, or WANDTs, namely *Waves that appear from nowhere and disappear without a trace* [31]) are now recognized as proper nonlinear structures. Research interest has by now advanced beyond the standard ocean-dynamical problem, tracing rogue waves in nonlinear optics [32–34], in superfluidity [35], in hydrodynamics [36], in atmospheric dynamics [37] and even in econophysics [38, 39].

In this study, we shall focus on rogue wave formation by means of nonlinear amplitude modulation of ion-acoustic wavepackets in an e–p–i plasma. We adopt a quantum approach by incorporating the Fermi statistics of both electrons and positrons in the description. Parameters entering the model include the electron to positron temperature ratio and the ionic Fermi to thermal pressure ratio. In section 2, an analytical fluid model is introduced. In section 3, a multiscale perturbation technique is outlined, modeling the evolution of the electrostatic potential (amplitude). In section 4, the linear regime, obtained to first order in the perturbation parameter ϵ, is briefly discussed. The nonlinear evolution of a wavepacket's amplitude is described in section 5. The modulational stability profile of the electrostatic potential is analyzed in section 6, and is then studied in terms of relevant plasma parameters in section 7. Known analytical envelope-soliton solutions of the amplitude evolution equation are presented in section 8. The relation to known scenarios for rogue wave formation is discussed in section 9. Finally, our results are summarized in the concluding section 10.

2. Quantum ion-fluid model

We consider a three-component plasma consisting of positive ions, electrons and positrons. A one-dimensional geometry is adopted, for simplicity. We are interested in studying the evolution of electrostatic excitations at the ion scale, assuming electrons and positrons constitute a homogeneous Fermi–Dirac-distributed background. The ions are subject to the Fermi pressure, a statistical effect associated with particles with a significant overlap in position wavefunction. The ion-fluid pressure is thus given by [2]

$$P = E_{\mathrm{Fi}} n_{\mathrm{i0}} \left(\frac{n_{\mathrm{i}}}{n_{\mathrm{i0}}} \right)^3 \tag{1}$$

where E_{Fi} is the ion Fermi energy, n_{i} is the ion number density and n_{i0} is the ion number density at equilibrium. The ion Fermi energy is given by $E_{\mathrm{Fi}} = \hbar^2 (3\pi^2 n_{\mathrm{i}})^{\frac{2}{3}} / 2m_{\mathrm{i}}$, where $\hbar$ is the scaled Planck's constant and m_{i} is the ion's mass. It is evaluated at the asymptotic value of density wherever it is encountered throughout this work. The electron/positron Fermi energy is given in similar fashion by $E_{\mathrm{Fe/p}} = \hbar^2 (3\pi^2 n_{\mathrm{e/p}})^{\frac{2}{3}} / 2m_{\mathrm{e/p}}$. The electron/positron number density is expressed as [42]

$$n_{\mathrm{e/p}} = -\left(\frac{m_{\mathrm{e/p}} k_{\mathrm{B}} T_{\mathrm{e/p}}}{2^{\frac{1}{3}} \pi \hbar^2} \right)^{\frac{3}{2}} Li_{\frac{3}{2}}(-\mathrm{e}^{\frac{\mathrm{e}\phi + \mu_{\mathrm{e0/p0}}}{k_{\mathrm{B}} T_{\mathrm{e/p}}}}), \tag{2}$$

where m_{e} is the electron mass, k_{B} is Boltzmann's constant, T_{e} is the electron temperature, μ_{e0} is the equilibrium electron chemical potential, e the elementary charge and ϕ the scalar potential. Quantities with a subscript 'p' refer to the equivalent for positrons. $Li_{\frac{3}{2}}$ denotes the polylogarithm function, arising from the integration of the Fermi–Dirac distribution. The polylogarithm can be defined in a recursive manner [43]:

$$Li_{s+1}(x) = \int_0^x \mathrm{d}y \frac{Li_s(y)}{y}. \tag{3}$$

The above model is a simpler version of the one discussed in [42]. It applies to very dense environments where ions, electrons and positrons are highly degenerate. Besides, electrons and positrons are described by the equilibrium Fermi–Dirac distribution, while ions are cold so that a zero-temperature Fermi gas equation of state applies. In the case of a nondegenerate plasma, this model would be formulated in terms of a classical equation of state for the ion fluid pressure, while electrons and positrons would be thermalized to Maxwell–Boltzmann equilibria.

The fluid (continuity and momentum) equations for the ions, coupled to Poisson's equation, are thus expressed as

$$\frac{\partial n_\mathrm{i}}{\partial t}+\frac{\partial (n_\mathrm{i} v_\mathrm{i})}{\partial x}=0, \tag{4}$$

$$\frac{\partial v_\mathrm{i}}{\partial t}+v_\mathrm{i}\frac{\partial v_\mathrm{i}}{\partial x}=-\frac{Z_\mathrm{i} e}{m_\mathrm{i}}\frac{\partial \phi}{\partial x}-\frac{n_{\mathrm{i}0}}{n_\mathrm{i} m_\mathrm{i}}E_\mathrm{Fi}\frac{\partial}{\partial x}\left(\frac{n_\mathrm{i}}{n_{\mathrm{i}0}}\right)^3, \tag{5}$$

$$\frac{\partial^2 \phi}{\partial x^2}=\frac{e}{\epsilon_0}(n_\mathrm{e}-n_\mathrm{p}-n_\mathrm{i} Z_\mathrm{i}), \tag{6}$$

where v_i is the ion velocity field, ϵ_0 is the vacuum permittivity and $Z_\mathrm{i} e$ is the ionic charge. For ions, due to their larger mass, quantum diffraction effects are fully negligible. Regarding electrons and positrons, only quantum statistical effects were taken into account, which is correct for highly degenerate plasma [42].

At equilibrium, the total (algebraic value of the) electric charge should vanish, so that $n_{\mathrm{e}0}-n_{\mathrm{p}0}-n_\mathrm{i} Z_\mathrm{i}=0$. Introducing the parameter $\beta=n_{\mathrm{p}0}/Z_\mathrm{i} n_{\mathrm{i}0}$, representing the ratio of positron charge density to the ion charge density, one may cast Poisson's equation in the form

$$\frac{\partial^2 \phi}{\partial x^2}=\frac{e n_{\mathrm{i}0} Z_\mathrm{i}}{\epsilon_0}\left(\frac{n_{\mathrm{e}0}}{n_{\mathrm{i}0} Z_\mathrm{i}}\frac{n_\mathrm{e}}{n_{\mathrm{e}0}}-\frac{n_{\mathrm{p}0}}{n_{\mathrm{i}0} Z_\mathrm{i}}\frac{n_\mathrm{p}}{n_{\mathrm{p}0}}-\frac{n_\mathrm{i}}{n_{\mathrm{i}0}}\right) \tag{7}$$

$$=\frac{e n_{\mathrm{i}0} Z_\mathrm{i}}{\epsilon_0}\left((1+\beta)\frac{n_\mathrm{e}}{n_{\mathrm{e}0}}-\beta\frac{n_\mathrm{p}}{n_{\mathrm{p}0}}-\frac{n_\mathrm{i}}{n_{\mathrm{i}0}}\right). \tag{8}$$

We proceed by scaling the number densities by their respective equilibrium values, expanding the power series expression of the polylogarithm functions (see above) and rescaling time, ion-fluid speed, potential and length by characteristic scales T_0, V_0, ϕ_0 and L_0 $(=V_0 T_0)$ respectively (to be defined at a later stage). The model equations are thus given in a dimensionless form by

$$\frac{\partial n}{\partial t}+\frac{\partial (nv)}{\partial x}=0, \tag{9}$$

$$\frac{\partial v}{\partial t}+v\frac{\partial v}{\partial x}=-a\frac{\partial \phi}{\partial x}-gn\frac{\partial n}{\partial x}, \tag{10}$$

$$\frac{\partial^2 \phi}{\partial x^2}\approx b(1-n)+c_1\phi+c_2\phi^2+c_3\phi^3. \tag{11}$$

The subscript 'i' has been dropped as it is clear that density and speed now relate to ions only. The (dimensionless) parameters appearing in the latter system are defined by

$$a=\frac{e Z_\mathrm{i}\phi_0 T_0}{L_0 V_0 m_\mathrm{i}}=\frac{Z_\mathrm{i} e\phi_0}{m_\mathrm{i} V_0^2}, \tag{12}$$

$$g=\frac{3E_\mathrm{Fi}}{m_\mathrm{i} V_0^2}, \tag{13}$$

$$b=\frac{e Z_\mathrm{i} n_{\mathrm{i}0} L_0^2}{\epsilon_0\phi_0}=L_0^2\frac{e^2 Z_\mathrm{i}^2 n_{\mathrm{i}0}}{\epsilon_0 Z_\mathrm{i} e\phi_0}, \tag{14}$$

$$c_j=\frac{b(1+\beta)}{j!Li_{\frac{3}{2}}(-\mathrm{e}^{\frac{\mu_{\mathrm{e}0}}{k_\mathrm{B}T_\mathrm{e}}})}\left(\frac{e\phi_0}{k_\mathrm{B}T_\mathrm{e}}\right)^j Li_{\frac{3}{2}-j}(-\mathrm{e}^{\frac{\mu_{\mathrm{e}0}}{k_\mathrm{B}T_\mathrm{e}}}),$$
$$-\frac{b\beta}{j!Li_{\frac{3}{2}}(-\mathrm{e}^{\frac{\mu_{\mathrm{p}0}}{k_\mathrm{B}T_\mathrm{p}}})}\left(\frac{-e\phi_0}{k_\mathrm{B}T_\mathrm{p}}\right)^j Li_{\frac{3}{2}-j}(-\mathrm{e}^{\frac{\mu_{\mathrm{p}0}}{k_\mathrm{B}T_\mathrm{p}}}). \tag{15}$$

The above expression for c_j is obtained by a Taylor expansion of the electron and positron densities about $\phi=0$. As the argument of the polylogarithm is exponential in ϕ, differentiation with respect to ϕ takes the form

$$\frac{\mathrm{d}}{\mathrm{d}\phi}Li_{\frac{3}{2}}(-\mathrm{e}^{\frac{e\phi+\mu}{k_\mathrm{B}T}})=\frac{e}{k_\mathrm{B}T}\xi\frac{\mathrm{d}}{\mathrm{d}\xi}Li_{\frac{3}{2}}(-\mathrm{e}^{\frac{e\phi+\mu}{k_\mathrm{B}T}})|_{\xi=-\mathrm{e}^{\frac{e\phi+\mu}{k_\mathrm{B}T}}},$$
$$\frac{\mathrm{d}}{\mathrm{d}\phi}=\frac{e}{k_\mathrm{B}T}\xi\frac{\mathrm{d}}{\mathrm{d}\xi}. \tag{16}$$

In conjunction with the recursive definition of the polylogarithm (3), successive applications of this derivative operator have the form

$$\left(\frac{\mathrm{d}}{\mathrm{d}\phi}\right)^n Li_{\frac{3}{2}}(-\mathrm{e}^{\frac{e\phi+\mu}{k_\mathrm{B}T}})=\left(\frac{e}{k_\mathrm{B}T}\right)^n Li_{\frac{3}{2}-n}(-\mathrm{e}^{\frac{e\phi+\mu}{k_\mathrm{B}T}}). \tag{17}$$

As it stands, L_0, T_0 and V_0 are completely arbitrary, as long as they are typical physical scales. However, if we assume, as in customary with classical plasmas, that $m_\mathrm{i} V_0^2$ is a measure of the (ion) thermal energy one will have $g\gg 1$, since the Fermi energy is much larger than the thermal energy. Since we have a degenerate plasma, the scaling must correspond to the Fermi energy.

The equations to be scaled are the ion equations. Taking into account the Fermi statistics, it is appropriate to define L_0, T_0 and V_0 with reference to the typical ion scales:

$$V_0=\left(\frac{2E_\mathrm{Fe}}{m_\mathrm{i}}\right)^{1/2}$$

and

$$L_0=\left(\frac{2\epsilon_0 E_\mathrm{Fe}}{3n_{\mathrm{i}0}Z_\mathrm{i}^2 e^2}\right)^{1/2}.$$

Note that V_0 is the formal equivalent of the ion-acoustic 'sound' speed in the classical description [16, 40, 41].

The appropriate quantum scales are given:

$$g=\frac{3E_\mathrm{Fi}}{2E_\mathrm{Fe}}=\frac{3}{2}\left(\frac{m_\mathrm{i}}{m_\mathrm{e}}\right)\left(\frac{n_{\mathrm{i}0}}{n_{\mathrm{e}0}}\right)^{\frac{2}{3}}=\frac{3m_\mathrm{e}}{2m_\mathrm{i}}\frac{1}{(Z_\mathrm{i}(1+\beta))^{\frac{2}{3}}},$$

$$a=\frac{Z_\mathrm{i} e\phi_0}{2E_\mathrm{Fe}},$$

$$b=\frac{2E_\mathrm{Fe}}{3Z_\mathrm{i} e\phi_0}=\frac{1}{3a},$$

$$c_j=\frac{b(1+\beta)}{j!Li_{\frac{3}{2}}(-\mathrm{e}^{\frac{\mu_{\mathrm{e}0}}{k_\mathrm{B}T_\mathrm{e}}})}\left(\frac{2E_\mathrm{Fe}}{3bZ_\mathrm{i}k_\mathrm{B}T_\mathrm{e}}\right)^j Li_{\frac{3}{2}-j}(-\mathrm{e}^{\frac{\mu_{\mathrm{e}0}}{k_\mathrm{B}T_\mathrm{e}}})$$
$$-\frac{b\beta}{j!Li_{\frac{3}{2}}(-\mathrm{e}^{\frac{\mu_{\mathrm{p}0}}{k_\mathrm{B}T_\mathrm{p}}})}\left(\frac{-2E_\mathrm{Fe}}{3bZ_\mathrm{i}k_\mathrm{B}T_\mathrm{p}}\right)^j Li_{\frac{3}{2}-j}(-\mathrm{e}^{\frac{\mu_{\mathrm{p}0}}{k_\mathrm{B}T_\mathrm{p}}}). \tag{18}$$

The contribution of the electrons to c_j through the polylogarithm terms can be expressed in terms of the ratios of their equilibrium number densities and their temperatures. Provided the temperature is low (i.e. $T_e < T_{Fe}$), the chemical potential of the electrons at equilibrium can be approximated by the Sommerfeld expansion:

$$\frac{\mu_{e0}}{k_B T_e} \approx \frac{E_{Fe0}}{k_B T_e} - \frac{\pi^2}{12}\frac{k_B T_e}{E_{Fe0}} - \frac{\pi^4}{36}\left(\frac{k_B T_e}{E_{Fe0}}\right)^3. \quad (19)$$

We note that, in fact, although the Fermi–Dirac distribution is valid for arbitrary temperatures, the Sommerfeld expansion is not. The Sommerfeld expansion of the positron chemical potential is

$$\frac{\mu_{p0}}{k_B T_p} \approx \frac{E_{Fp0}}{k_B T_p} - \frac{\pi^2}{12}\frac{k_B T_p}{E_{Fp0}} - \frac{\pi^4}{36}\left(\frac{k_B T_p}{E_{Fp0}}\right)^3. \quad (20)$$

The ratio, $k_B T_p/E_{Fp0}$ must be much less than unity for this truncation of the Sommerfeld expansion to be a good approximation. However, $E_{Fp0} = (\beta/1+\beta)^{\frac{2}{3}} E_{Fe0} \sim \beta^{\frac{2}{3}} E_{Fe0}$ (for $\beta \ll 1$), so for $\beta \lesssim (k_B T_e/E_{Fe0})^{\frac{3}{2}}$ the Sommerfeld expansion is divergent unless the positron temperature is reduced accordingly. The physical content of this is that if the density is so low that $k_B T_p \gg E_{Fp0}$, then the positrons behave as a classical gas.

It can be seen that charge screening is introduced by c_1, which is positive. Nonlinearity is taken into account by c_2 and c_3, all of which depend on the electron and positron temperatures. We spell out, for later reference, the expression for c_1,

$$c_1 = \frac{b(1+\beta)}{Li_{\frac{3}{2}}(-e^{\frac{\mu_{e0}}{k_B T_e}})}\left(\frac{2E_{Fe}}{3bZ_i k_B T_e}\right) Li_{\frac{1}{2}}(-e^{\frac{\mu_{e0}}{k_B T_e}}) + \frac{b\beta}{Li_{\frac{3}{2}}(-e^{\frac{\mu_{p0}}{k_B T_p}})}\left(\frac{-2E_{Fe}}{3bZ_i k_B T_p}\right) Li_{\frac{1}{2}}(-e^{\frac{\mu_{p0}}{k_B T_p}}), \quad (21)$$

which is associated with charge screening effects and determines the sound speed for electrostatic waves.

3. Multiple scales perturbation

We assume each of n, v and ϕ takes the form of a modulated envelope—i.e. the composition of a fast carrier wave with a slow variation in amplitude. We then declare that the carrier depends on (x, t), but the wave envelope depends on an infinite set of variables, $\{X_1, X_2, \ldots, T_1, T_2, \ldots\}$, where $T_r = \epsilon^r t$ and $X_r = \epsilon^r x$ (for $r = 1, 2, 3, \ldots$) and $\epsilon \ll 1$ is a free (real, small) parameter. Furthermore, the variables are expanded around their equilibrium values:

$$\begin{aligned} n &\approx 1 + \epsilon n_1 + \epsilon^2 n_2 + \cdots, \\ v &\approx \epsilon v_1 + \epsilon^2 v_2 + \cdots, \\ \phi &\approx \epsilon\phi_1 + \epsilon^2\phi_2 + \cdots. \end{aligned} \quad (22)$$

Each of these u_j (say, any of n_j, v_j, ϕ_j) is split into a sum of Fourier components:

$$u_j = \sum_{r=-j}^{j} u_j^{(r)} e^{ir(kx-\omega t)}. \quad (23)$$

The number density, speed and potential are real-valued quantities, so $u_j^{(-r)} = \bar{u}_j^{(r)}$ (the bar here denoting the complex conjugate). The stretched variables are treated as independent variables. After feeding the above information into the model equations, one obtains a set of vanishing polynomials in ϵ. Since ϵ is a free parameter, the coefficients of ϵ must vanish. Solving at successive orders provides a solution for the state variables, in terms of their harmonic amplitudes. This is essentially the long established method of multiple scales of Taniuti and Yajima [15], applied to the case of electrostatic plasma waves [16].

4. Linear analysis

The equations in the first order of ϵ can be expressed in the form of a singular matrix equation, the operator of the equation possessing a nontrivial kernel. The vanishing determinant of this operator forms the dispersion relation

$$\omega^2 = \frac{k^2 ab}{k^2 + c_1} + gk^2, \quad (24)$$

The three linear equations in ϕ_1, n_1 and v_1 are underdetermined, so letting the electric potential (amplitude) $\phi_1^{(1)} = \psi$ be a free variable, we obtain:

$$\phi_1 = \psi e^{i(kx-\omega t)} + \bar{\psi} e^{-i(kx-\omega t)}, \quad (25)$$

$$n_1 = \frac{c_1 + k^2}{b}\phi, \quad (26)$$

$$v_1 = \frac{\omega}{k}\frac{c_1 + k^2}{b}\phi. \quad (27)$$

A few comments are in order, regarding the dispersion relation (24). First of all, we note that, taking into account (18), (24) takes the form

$$\omega^2 = \frac{k^2}{3(k^2 + c_1)} + gk^2. \quad (28)$$

Recall that the quantity c_1, given by (18) above as a function of the plasma configuration (density and temperature ratios), is essentially related with the charge screening mechanism in this model, and in fact affects the phase speed. We note that the phase speed $v_{ph} = \omega/k \simeq \sqrt{ab/c_1 + g}$ for large wavelength values (small wavenumber k). Therefore, the phase speed is modified by both the electron and positron statistics (via c_1) and the Fermi pressure (via g). On the opposite limit of ultrashort wavelengths (large k), v_{ph} tends to the constant g (here recovering the quantum equivalent of ion thermal waves) or to zero (namely, $\omega \to (ab)^{1/2}$, or $\omega/k \to 0$), if the Fermi pressure were to be neglected (setting $g = 0$). Let us point out that, although we kept the dispersion relation (24) above in its general form, the coefficients appearing in it are prescribed as $ab = 1/3$ for our scaling adopted in the previous section. Therefore, the dependence on the plasma configuration (effect of β and of the positron-to-electron temperature ratio, namely) will appear only through c_1 (recall the definitions (18) above) and also via g, whose contribution is of order no greater than 10^{-3}.

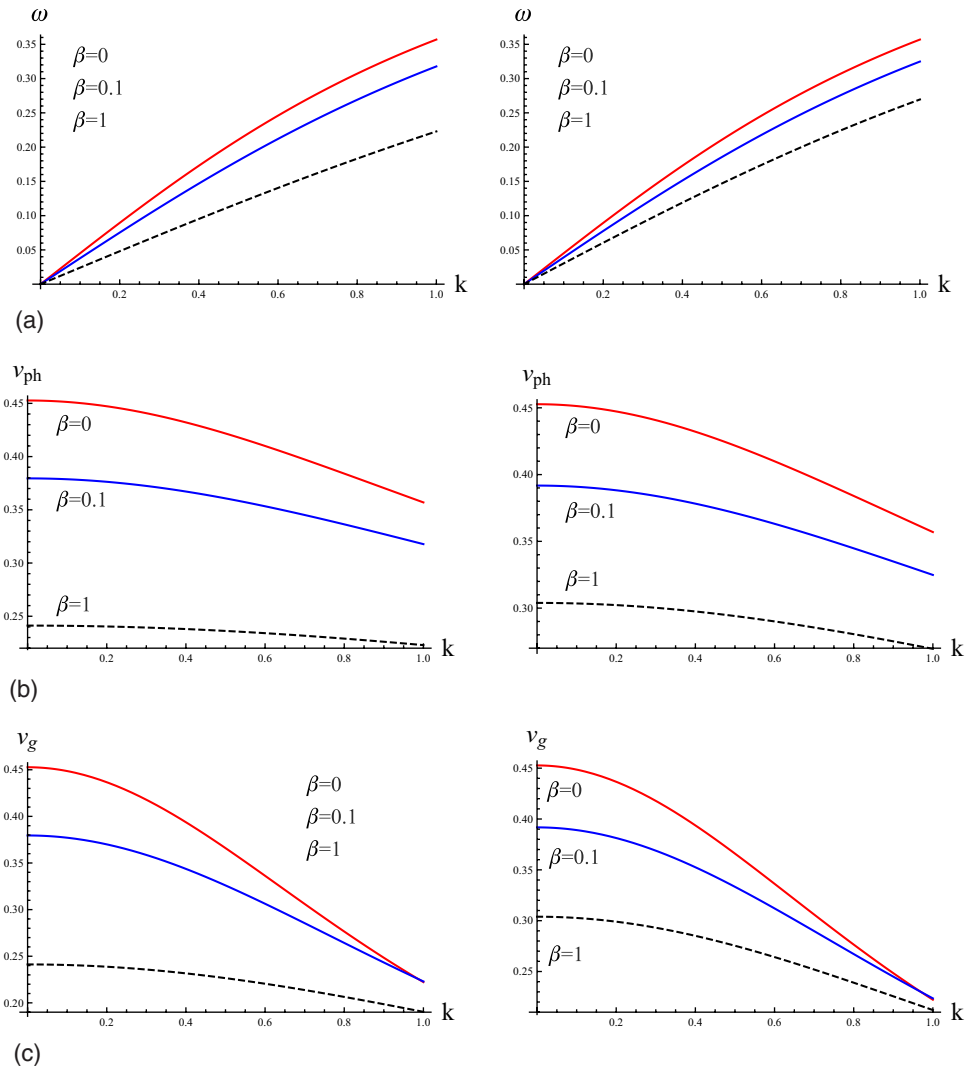

Figure 1. Illustrative plots of the frequency, the phase speed, $v_{\rm ph} = \omega/k$, and the group velocity, $v_g = {\rm d}\omega/{\rm d}k$, versus the wavenumber k, for different values of the positron–ion charge density ratio, β. The parameter values in this plot have been arbitrarily chosen so that $ab = 1/3$, $n_{\rm i0} = 10^{33}$ and $T_{\rm e} = T_{\rm p} = 10^7$ K. The plots to the right are made with fixed scales (corresponding to a reference density $n_{\rm e} = 10^{33}\,{\rm m}^{-3}$; see discussion in section 7).

Therefore, the quantitative effect of β (and of the positron-to-electron temperature ratio) on the dispersion characteristics will admittedly be rather weak, though measurable, as depicted in figures 1 and 2.

Figure 1 depicts the frequency, phase speed (ω/k) and group velocity (${\rm d}\omega/{\rm d}k$). For each plot, the curves for different values of the positron–ion charge density ratio converge rapidly to the same asymptote. The expression for the group velocity is given in the next section.

Figure 2 provides the same functions, but for different positron temperatures. The effect of the positron temperature on the wave frequency is much weaker than that of the charge density ratio, β.

5. Nonlinear amplitude dynamics

The equations of second order yield expressions for the zeroth, first and second harmonics. We will summarize the obtained results below, omitting unnecessary details.

The equations for the first-harmonic components force a condition on the speed of the envelope:

$$\frac{\partial\psi}{\partial T_1} + v_g\frac{\partial\psi}{\partial X_1} = 0 \tag{29}$$

where we have defined the group velocity $v_g = {\rm d}\omega/{\rm d}k = (abc_1/(c_1+k^2)^2 + g)k/\omega$ (see figure 1). In account of the latter constraint, we assume that the envelope moves at the group velocity, namely $\psi = \psi(X_1 - v_g T_1, X_2, T_2, \ldots))$.

As with the first-order case, the indeterminacy in the linear system requires the introduction of another arbitrary function, φ. This, however, can be neglected for physical reasons, backed up by its self-exclusion in the final evolution equation. The first-harmonic component of ϕ can be written: $\epsilon(\psi + \epsilon\varphi){\rm e}^{{\rm i}(kx-\omega t)}$, so φ is an infinitesimal correction to ψ and can thus be ignored. Nevertheless, it will be left in for the sake of completeness:

$$\phi_2^{(1)} = \varphi, \tag{30}$$

$$n_2^{(1)} = \frac{c_1 + k^2}{b}\varphi - \frac{2{\rm i}k}{b}\frac{\partial\psi}{\partial X_1}, \tag{31}$$

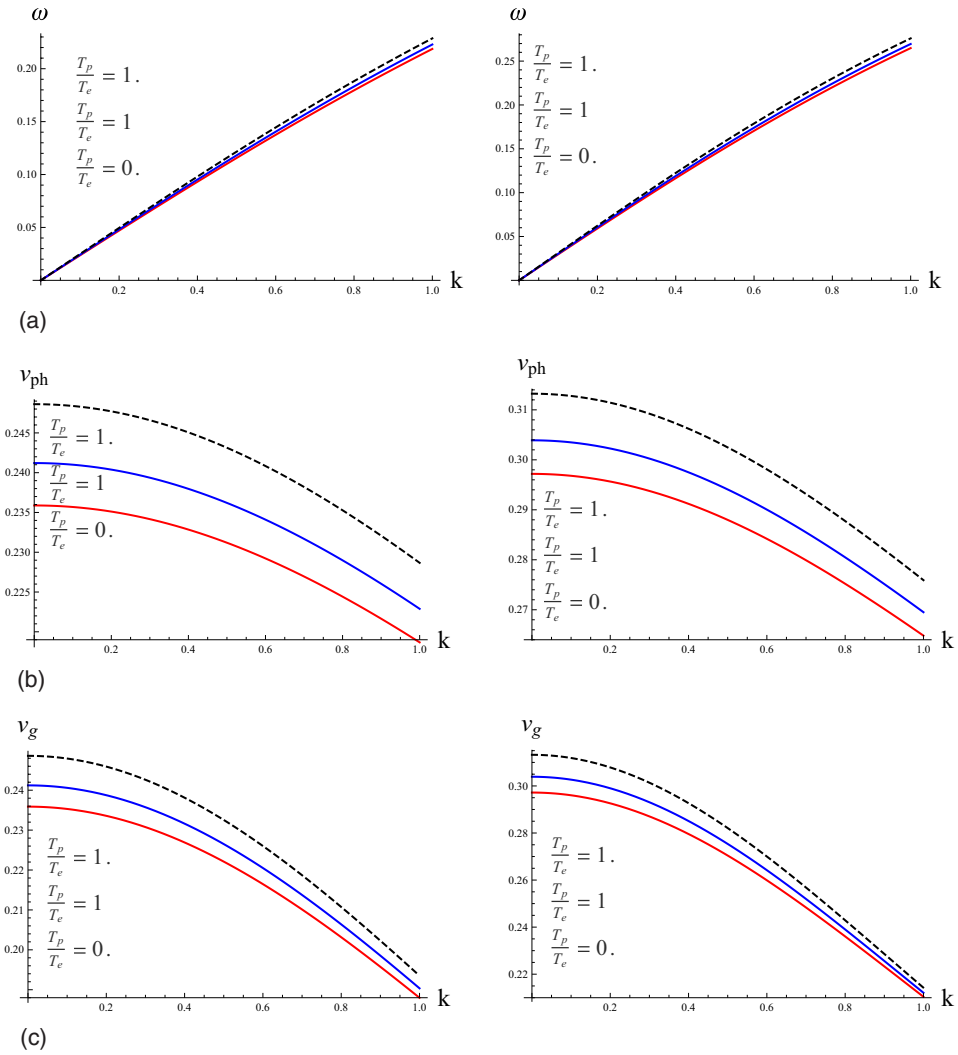

Figure 2. Illustrative plots of the frequency, the phase speed and the group velocity, versus the wavenumber for different positron temperatures with fixed electron temperature. The parameter values in this plot have been arbitrarily chosen so that $ab = 1/3$, $n_{i0} = 10^{33}$, $T_e = 10^7$ K and $\beta = 1$. The plots to the right are made with fixed scales (corresponding to a reference density $n_e = 10^{33}\,\mathrm{m}^{-3}$; see discussion in section 7).

$$v_2^{(1)} = \frac{\omega}{k}\frac{c_1 + k^2}{b}\varphi + \mathrm{i}\frac{c_1 + k^2}{b}\left(\frac{\omega}{k^2} - \frac{v_g}{k} - \frac{2\omega}{c_1 + k^2}\right)\frac{\partial\psi}{\partial X_1}. \tag{32}$$

The second harmonic components are found to be proportional to ψ^2, while the zeroth harmonics are proportional to $|\psi|^2$, as expected [16]. Detailed expressions for the coefficients are provided in the appendix. It may be noted that the zeroth harmonics are not entirely obtained from the second-order equations, so one needs to resort to the third-order equations for these to be determined.

The third-order equations also yield an evolution equation for ψ as a consequence of the singular operator in the first-harmonic equations. In other words, a series of secular terms arises in the right-hand side, if one considers the first-harmonic contribution, entering in resonance with the null space of the first-order operator defined in the first order. This contribution must be forced to vanish, otherwise the solution will diverge in time. The condition for annihilation of secular terms leads precisely to a partial-differential equation for the electrostatic potential envelope (amplitude), ψ, which takes the form of a NLSE:

$$\mathrm{i}\frac{\partial\psi}{\partial\tau} + P\frac{\partial^2\psi}{\partial X_1^2} + Q|\psi|^2\psi = 0. \tag{33}$$

It is worth noting that the dispersion coefficient $P(k; g, c_1)$ is related to the dispersion relation, as $P = \frac{1}{2}\frac{\mathrm{d}^2\omega}{\mathrm{d}k^2}$: this recovers the expected result from nonlinear optics [18]. The nonlinearity coefficient Q, on the other hand, is a function of the wavenumber k and also incorporates the quantum effect via its dependence on $\{g, c_1, c_2, c_3\}$. The lengthy expressions for these coefficient is reported in the appendix.

It may be interesting to trace the analytical trend for small k (large wavelength) by deriving approximate expressions for $k \ll 1$. A straightforward McLaurin expansion leads us to the analytical relation

$$P \approx -\frac{3ab}{2c_1^2\sqrt{\frac{ab}{c_1} + g}}k \tag{34}$$

(where we have used the positivity of c_1, imposed as a linear stability requirement—see equation (24)—to simplify the latter expression). We see that P acquires negative values near $k \simeq 0$. On the other hand, Q behaves as $\sim k^{-1}$:

$$Q \approx \left[\frac{\frac{c_1^2}{2b}(3ab + 4c_1 g) - abc_2}{3ab} + \frac{1}{3a}(2ac_2 - \frac{c_1^2}{b^2}(3ab + 4gc_1)) \right] \times \frac{\sqrt{abc_1 + gc_1^2}}{b} \left[\frac{ab^2 c_2}{c_1^2(ab + gc_1)} - 1 - \frac{c_1}{2(ab + gc_1)} \left(\frac{ab}{c_1} + 2g \right) \right] \frac{1}{k}. \quad (35)$$

Details are given in the appendix.

It is noted that $P < 0 < Q$ near $k \simeq 0$, thus ensuring stability of the envelope (for any parameter values), as we shall see in the next section.

6. Modulational stability analysis

Let us adopt a reference solution, $\psi_0 = a_0 e^{i Q a_0^2 \tau}$ and let us disturb this solution with two small, real functions, a_1 and b_1:

$$\psi_0 \mapsto (a_0 + a_1) e^{i(Q a_0^2 + b_1)} \quad (36)$$

with $a_1 \ll a_0$, $b_1 \ll Q a_0^2$ and $O(\frac{a_1}{b_1}) \sim 1$. Since the disturbances are real, the resulting equation can be split easily into a real component and an imaginary component, which constitute a pair of simultaneous equations for a_1 and b_1:

$$\begin{aligned} -b_{1\tau} + P a_{1xx} + 2Q a_0^2 a_1 = 0, \\ a_{1\tau} + P b_{1xx} = 0. \end{aligned} \quad (37)$$

If the disturbance is periodic, then $a_1 = A e^{i(\kappa x - \Omega \tau)}$, $b_1 = B e^{i(\kappa x - \Omega \tau)}$ with A and B complex. κ and Ω are respectively the perturbation wavenumber and frequency. This allows the above equations to take a convenient matrix form:

$$\begin{pmatrix} 2Q a_0^2 - P\kappa^2 & i\Omega \\ -i\Omega & -P\kappa^2 \end{pmatrix} \begin{pmatrix} A \\ B \end{pmatrix} = \begin{pmatrix} 0 \\ 0 \end{pmatrix}. \quad (38)$$

The determinant of this matrix must vanish, which yields a dispersion relation for the perturbation:

$$\Omega^2 = (P\kappa^2)^2 \left(1 - \frac{2Q a_0^2}{P\kappa^2} \right). \quad (39)$$

When $PQ > 0$, the frequency becomes imaginary and so the perturbed function can grow or decay exponentially. The threshold for instability is given by

$$\kappa_{crit} = a_0 \sqrt{\frac{2Q}{P}}, \quad (40)$$

values of κ below this give rise to instability. The growth rate attains its maximum at $\kappa_{max} = a_0 \sqrt{\frac{Q}{P}}$.

The mechanism discussed in this section is tantamount to a Benjamin–Feir-type instability in hydrodynamics [16, 18].

7. Parametric analysis

We have seen that the relevant plasma configurational parameters enter the dynamics via the analytical relations obtained above, and in particularly through the definition of coefficients P and Q; apart from the carrier wavenumber k and the associated frequency $\omega(k)$, these are the positron concentration (via the ratio $\beta = n_{p0}/(Z_i n_{i0})$), the electron and positron temperatures, T_e and T_p (entering (15)) and the Fermi energy (via g). We now plan to investigate the effect of these parameters on the modulational stability profile, as well as on the dynamics of localized excitations.

We proceed by selecting appropriate scales (see section 2 above). For analytical convenience, we adopt the choice $a = b = 1/\sqrt{3}$ (that is, for given arbitrary parameter values, in account of (18) above (we shall assume $Z_i = 1$ throughout the rest of this section). Furthermore, we shall set (the perturbation amplitude in (38)–(40)) $a_0 = 1$ for numerical applications in the following. Electron and positron temperatures are taken as equal unless otherwise stated.

The plots provided herewith are based on a plasma with ionic particle density $n_{i0} \sim 10^{33}\,m^{-3}$ and a temperature, $T_e \sim 10^7$ K, typical, say, of a red dwarf star (corresponding to a density of $10^3\,g\,cm^{-3}$ [44]).

An important note is in row, at this stage, regarding the numerical investigation to follow. Although the scaling introduced above is convenient and physically transparent, it is difficult to compare plots for different parameter values since some of these parameters influence the scales. For example, L_0 depends both on n_{i0} and n_{e0} (through $e\phi_0 = E_{Fe0}$). A change in β should therefore affect either of them, via the relation $n_{e0} = (1+\beta)n_{i0}$, and this would affect the other scales in turn. With this in mind, some of the plots provided in the following have been accompanied by plots obtained for the same parameters, but scaled by fixed values (considering an arbitrary fixed 'reference plasma density'). In the specific case of figures 1–10, the scales take the same form except that we have considered in the place of E_{Fe} the Fermi energy of an electron cloud with $n_e = 10^{33}\,m^{-3}$, so that g is no longer dependent on β ($g = 3m_e/2m_i$). We resolve to keep n_{i0} fixed so that n_{e0} changes with β. As it turned out, the qualitative trends of the curves presented in our plots do not depend on the scaling (compare the left to right panels in all figures, to see this), although the quantitative values may differ. Therefore, we have chosen to present both version of the graphs, for clarity and comparison.

Figure 3 shows how the stability of the solutions changes for different positron densities. We recall that P is the dispersion coefficient, while Q is related to the self-interaction of the carrier wave. It can be seen that, for each value of the positron-to-ion charge density ratio, β (=$n_{p0}/(Z_i n_{i0})$), there are two points in k where $PQ = 0$. One of these roots corresponds to $Q = 0$ and the other occurs when $P = 0$. An increase in positron density, relative to ion density (i.e. increasing β), is tantamount to higher number of mobile electrons (namely, $n_{e0} = n_{p0} + Z_i n_{i,0}$). Instability takes place over a larger range of k, but also sets in at a higher minimum value. In other words, the instability window (in carrier wavenumbers) is extended by introducing more positrons, but the threshold is also increased.

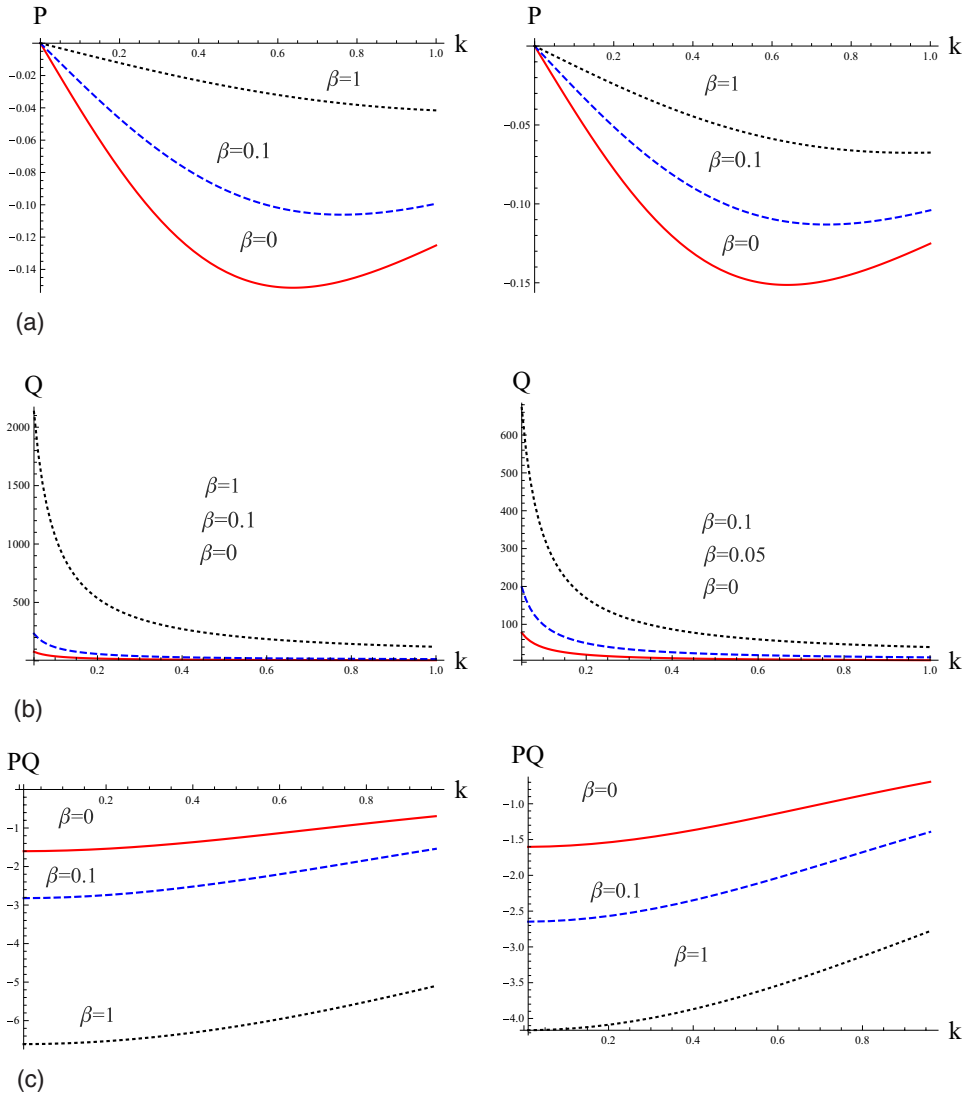

Figure 3. The effect of positron population ($\beta = \frac{n_{p0}}{n_{i0}Z_i}$) on P, Q and on their product PQ is shown above (with $T_e = T_p$), in (*a*), (*b*) and (*c*), respectively. Recall that the region $PQ > 0$ admits unstable harmonic (and stable bright-type envelope soliton) solutions of the NLSE. The plots to the right were made with a fixed scale (see discussion in section 7).

Figure 4 shows a similar set of plots, this time for different values of the positron-to-electron temperature ratio (and fixed density ratio). Decreasing this ratio with electron temperature fixed in this case increases both the instability threshold and its range in k. (The values on the plot are indicative, as one would expect positrons and electrons to be characterized by comparable temperature.)

An unstable wavepacket here exhibits exponential growth, characterized by a growth rate given by (39). This growth rate is plotted for a range of values of β (see figure 5) and positron temperatures (see figure 6).

The critical perturbation wavenumber κ_{crit}, given by (40), is plotted for different values of k over a range of positron–ion charge density ratios, β, in figure 7. Note that the solution is stable (κ_{crit} is imaginary) for β above a certain value when $k = 2.3$, which is verified by figure 8.

Let us see how positron concentration and temperature affect the range of values for k which allow for modulational instability to occur. The instability region is determined by the sign of PQ (while its root defines the relevant instability threshold): the product is initially negative, becoming positive as Q becomes negative and finally becoming negative as P becomes positive again. The instability carrier wavenumber k threshold, say k_{crit}, is therefore given by the root of Q (figure 9).

Let us now look at the effect of temperature and positron population on the charge shielding radius ('Debye length'), here associated with c_1, defined above. Figure 10 shows the variation of the screening radius with the positron–electron temperature ratio for different positron concentrations. As the temperature ratio increases, with the positrons becoming more energetic in comparison to the electrons, the shielding radius increases. An increase in the number of positrons has the opposite effect.

8. Envelope solitons

Various types of analytical solutions for the NLSE (33) have been obtained in the past. Focusing on space-localized

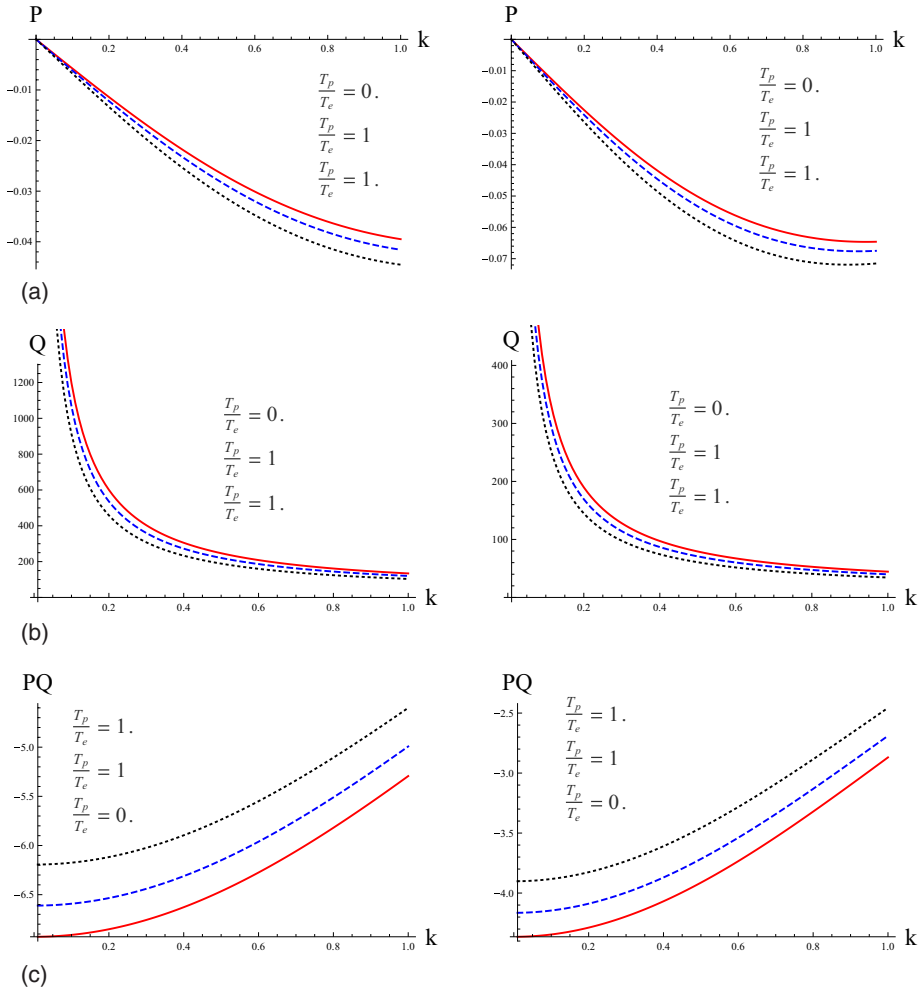

Figure 4. The effect of electron–positron temperature ratio on P, Q, PQ is shown above for $\beta = 1$. The curve in red shows Q with $T_p/T_e = 0.5$; the blue, dashed curve is for $T_p/T_e = 1$; and the black, dotted curve is for $T_p/T_e = 1.5$. The plots to the right were made with a fixed scale (see discussion in section 7).

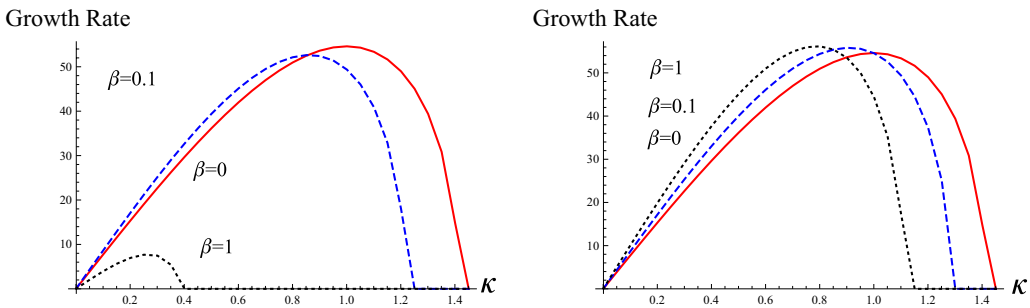

Figure 5. The modulational instability growth rate is depicted as a function of perturbation wavenumber, κ, for different values of β. Positron temperature is here equal to the electron temperature, κ is in units of κ_{max} for $\beta = 0$. $k = 3.5$ for all three curves. The plot to the right was made with a fixed scale (see discussion in section 7).

solutions of the envelope-soliton type, of particular importance here, let us briefly recall *bright-type* envelope (pulse) solitons and *gray-* or *dark*-type envelope solitons (holes) can exist in this system [18, 45–47]. In the following, we shall summarize relevant information on these solutions, before we proceed to an investigation of their characteristics in our physical problem.

The solutions of interest are found by setting $\psi = \rho e^{i\Theta}$, and then obtaining expressions for the nonlinear phase shift Θ and the envelope form ρ. Therefore, one distinguishes two components: an internal oscillation and an envelope formed by the variation in amplitude. In the remaining part of this Section, we omit analytical details, focusing on the qualitative aspects of the solutions. Details on the algebraic derivation of the fundamental envelope-soliton solutions can be found, e.g., in [16, 17, 47].

The bright soliton form represents an envelope pulse modulating an internal oscillation (see figure 11). Bright-type

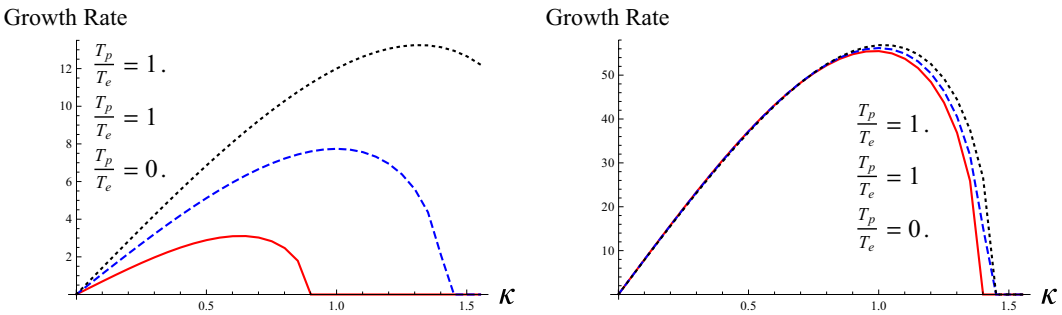

Figure 6. The modulational instability growth rate is depicted as a function of perturbation wavenumber, κ, for different positron temperatures. κ is in units of $\kappa_{\max}$ for $T_p = T_e$. $k = 3.5$ for all three curves. The plot to the right was made with a fixed scale (see discussion in section 7).

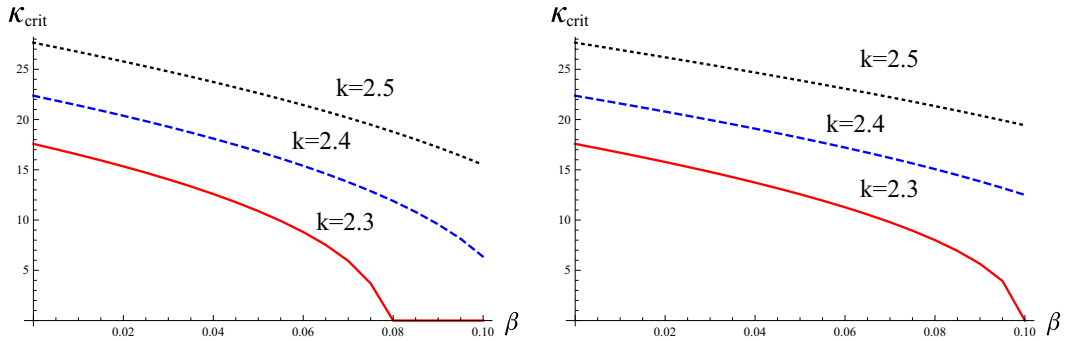

Figure 7. An increase in positron population affects the stability threshold (40) as shown above. The plot to the right was made with a fixed scale (see discussion in section 7).

envelope solitons exist for positive values of the PQ product, and are thus expected to occur in the large wavelength (small wavenumber) region; see figures discussed in the preceding section.

A different class of solitons, classified as either of *gray* or *dark* type, correspond to a propagating void (a *hole*) amidst a constant region. The *gray* soliton represents a local reduction in intensity in the medium through which it travels. The *dark* soliton is a traveling region of zero intensity; see figure 12. Dark-type envelope solitons exist for negative values of the PQ product, and are thus expected to occur for shorter wavelengths (larger wavenumbers) (again, the reader is referred to the plots presented in the preceding section).

9. Rogue waves

Rogue waves (or freak waves) are extreme events which occur in abundance in the ocean surface [21, 27, 48]. These are structures which may be localized (restricted) in both space and time domains. The term is earned by their behavior: a sudden appearance from an oscillating ambient background, accompanied by a narrowing of width and growth of amplitude far exceeding the 'average' background turbulence, followed by an equally rapid decay to the background medium [48, 49].

It was earlier suggested [50] that a class of breather-type solutions of the NLSE may be good candidates for modeling of rogue waves, as they capture the essential physics and the qualitative features of freak waves. In plasma physics, this is still a practically unexplored area, beyond a few first phenomenological investigations (see e.g. [51, 52]). In the following, we shall summarize the current state of the art, regarding analytical rogue-wave-like solutions of the NLSE (33), briefly discussing their relevance in our current context.

The Peregrine soliton. The Peregrine 'soliton' [49, 50] appears to be a good qualitative candidate for a freak-wave-like behavior based on a NLS description. A pioneering recent study has focused on the relevance of this solution in nonlinear optics [33], while its validity has been tested against controllable experimental observations in water basins [36]. Most interestingly, a first experimental observation of Peregrine solitons in plasmas has been reported [53], yet in restricted conditions which are far from being thoroughly understood.

The Peregrine solution reads:

$$\psi = \mathrm{e}^{\mathrm{i}Qt}\left[1 - \frac{4(1+2\mathrm{i}Qt)}{1+\frac{2Q}{P}x^2+4Q^2t^2}\right]. \qquad (41)$$

The corresponding waveform decays to a plane wave asymptotic background for either large x or t, but exhibits nontrivial behavior over a small region of (x, t); see figure 13. Obviously, for parametric investigation purposes, all physical information is contained within the coefficients P and Q in (41) (and (33)) which are functions of relevant plasma parameters.

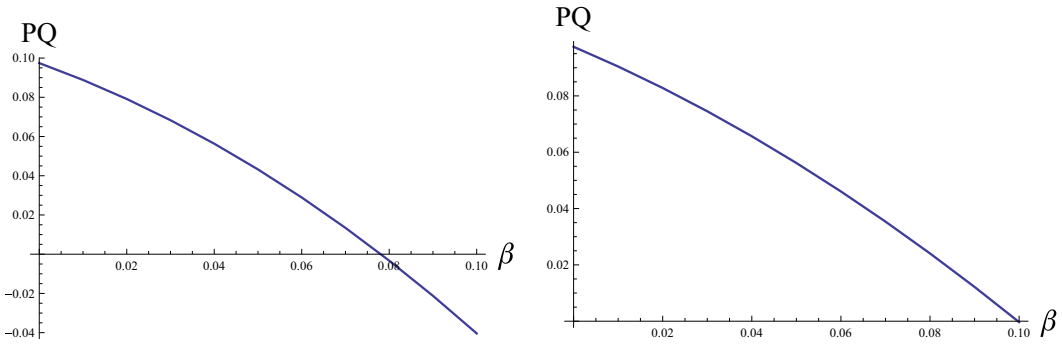

Figure 8. For large k ($k = 2.3$ in this plot), solutions are unstable for small β.

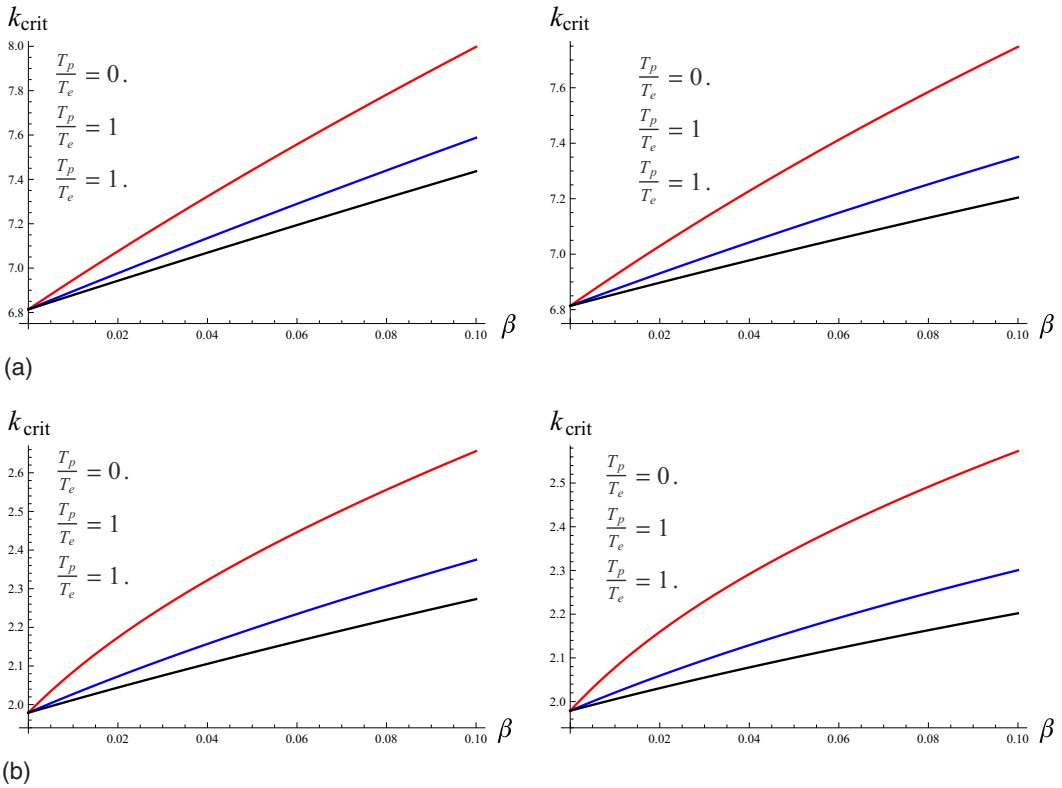

Figure 9. Plot of k_{crit} versus β for different values of the ratio T_e/T_p. (a) gives the upper bound on k, whereas (b) gives the lower bound on k. Between these bounds are the values of k which allow instability. The plots to the right were made with a fixed scale (see discussion in section 7).

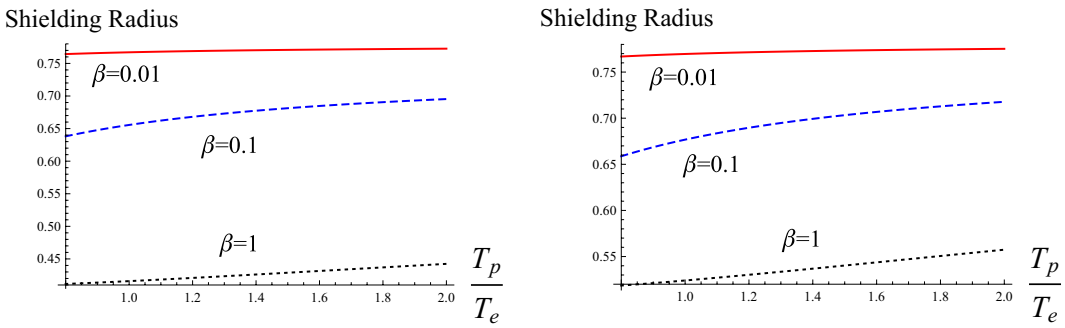

Figure 10. Debye radius ($\sim 1/\sqrt{c_1}$) versus electron–positron temperature ratio, T_e/T_p, for different values of β. The plot to the right was made with a fixed scale (see discussion in section 7).

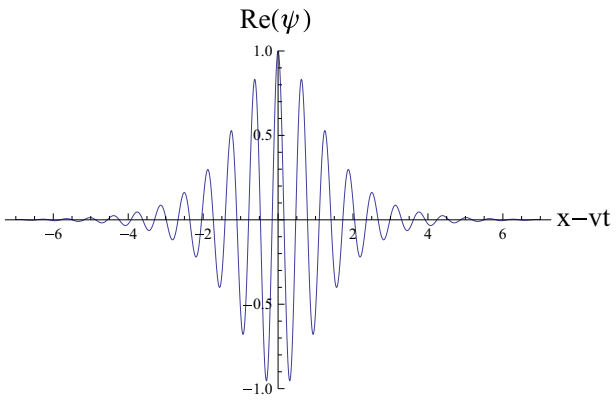

Figure 11. The *bright* envelope soliton amplitude varies roughly as $\mathrm{sech}(x - vt)$.

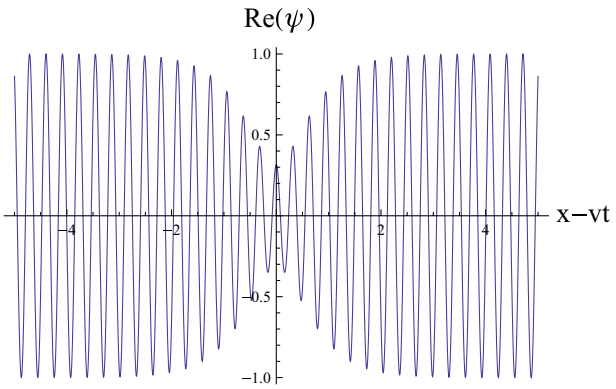

Figure 12. Heuristic plot of the *gray-type* envelope soliton, whose amplitude varies roughly as $[1 - d^2\mathrm{sech}^2(x - vt)]^{1/2}$. Setting $d = 1$ results in a *dark-type* envelope soliton.

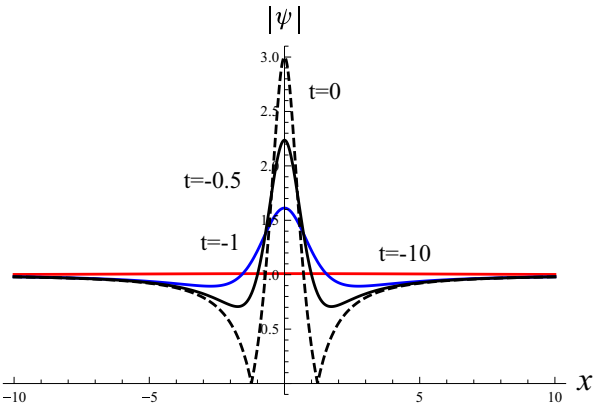

Figure 13. Plot of Peregrine's solution for different values of t. From (41), it can be seen that $|\psi|$ is an even function of t. The lump rises from a small, oscillating background for $t < 0$, reaches a peak amplitude and disappears again.

Akhmediev breather. Akhmediev's breather solution [50] is given by

$$\psi = \mathrm{e}^{\mathrm{i}Qt} \times \frac{\cosh(Q\sin(2\varphi)t - 2\mathrm{i}\varphi) - \cos(\varphi)\cos(2\sin(\varphi)\sqrt{\frac{Q}{2P}}x)}{\cosh(Q\sin(2\varphi)t) - \cos(\varphi)\cos(2\sin(\varphi)\sqrt{\frac{Q}{2P}}x)}. \tag{42}$$

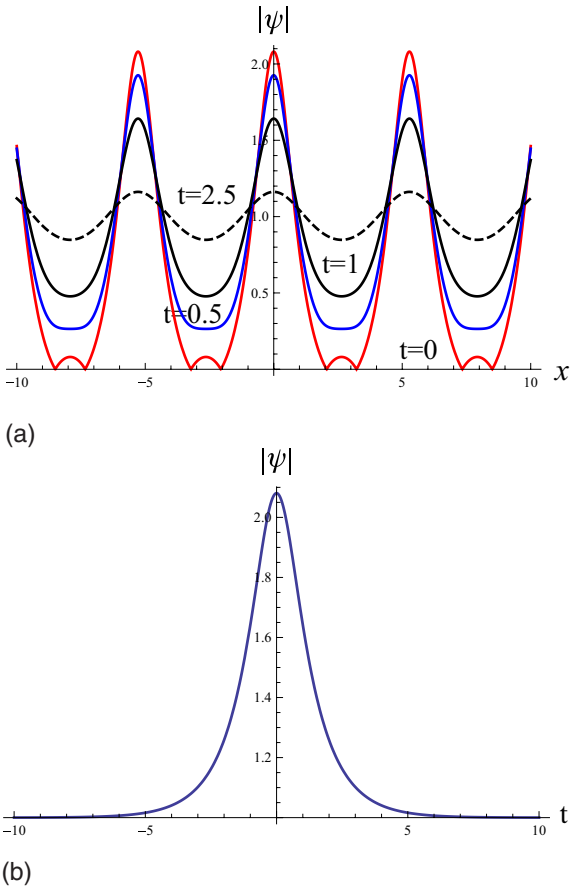

Figure 14. As suggested by (42), the Akhmediev breather is periodic in space, but not in time.

It is straightforward to see that this waveform is periodic in space only, while the Peregrine solution is recovered if one takes the limit of infinite spatial period.

Kuznetsov–Ma breather. The Kuznetsov–Ma breather, given by

$$\psi = \mathrm{e}^{\mathrm{i}Qt} \times \frac{\cos(Q\sinh(2\varphi)t - 2\mathrm{i}\varphi) - \cosh(\varphi)\cosh(2\sinh(\varphi)\sqrt{\frac{Q}{2P}}x)}{\cos(Q\sinh(2\varphi)t) - \cosh(\varphi)\cosh(2\sinh(\varphi)\sqrt{\frac{Q}{2P}}x)}, \tag{43}$$

is periodic in time only. Interestingly, the Peregrine solution is recovered if one takes the limit of infinite temporal period. Ma's soliton can be obtained from Akhmediev's (and vice versa) upon a formal phase shift, $\varphi \mapsto \pm\mathrm{i}\varphi$.

The reader will notice in that the asymptotic values of $\mathrm{Re}(\psi)$ oscillate over the range of t used. This is because both solutions decay to an exponential $\mathrm{e}^{\mathrm{i}Qt}$ in the limit of large x. The Kuznetsov–Ma soliton was derived with this as a boundary condition. It also follows directly from Peregrine's solution (41), which looks like its asymptotic function with a localized disturbance around $(0, 0)$. The quotient of a linear function of t and a quadratic function of both x and t must approach zero for large values of these variables. The graphs presented here in figures 13–15 were plotted with $P = Q = 1$ (heuristic *ad hoc* values).

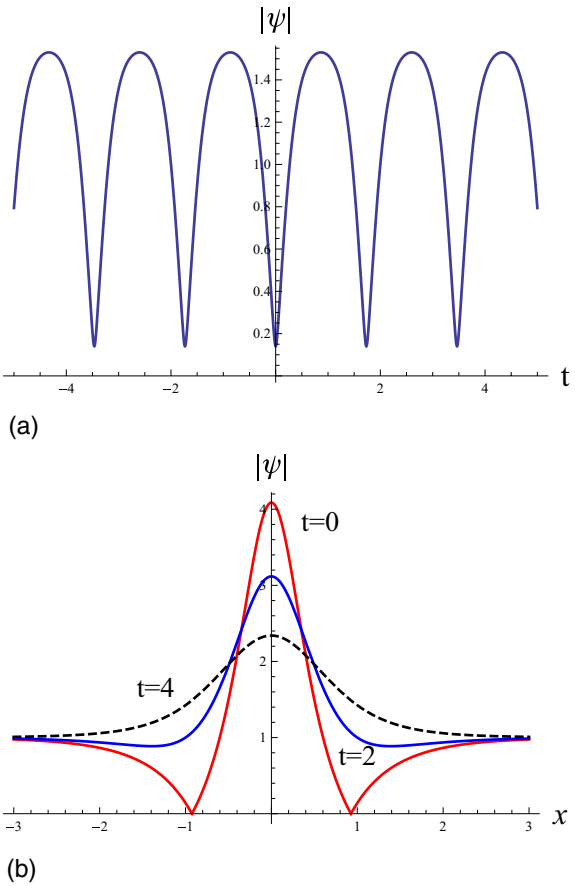

Figure 15. Equation (43) shows that Ma's breather is periodic in time, but not in space. (*a*) shows the variation of $|\psi|$ at the point $x = 0$ for $t \in [-10, 10]$. (*b*) shows how the breather is localized in space.

9.1. Parametric analysis

Plots of the above rogue waveforms against x and t are given in figures 16–18. In the first of these, the three types of analytical expressions presented above are depicted, adopting (*ad hoc*) values for $P = Q = \varphi = 1$, for illustrative purposes. The plots clarify the behavior of each type of excitation. These excitations are dependent on Q for their periodicity, so it is possible to 'tune' the parameters of the plasma for to obtain a particular character of rogue wave.

In figure 17, Peregrine's soliton with $\beta = 0$ is compared with that with $\beta = 0.1$. The duration of the excitation is seen to increase in both space and time. In figure 18, the solution with $T_p = 0.5T_e$ is compared with that which has $T_p = 1.5T_e$. The duration is greater with lower positron temperature.

A similar set of plots are presented (see figure 19) to show the effect of β and T_p/T_e on the waveform. As might be expected, Akhmediev's solution shares some of the traits of Peregrine's solution, but also displays new behavior due to its periodicity. An increase in β results in a wave that is less localized, so its frequency decreases. On the other hand, an increase in T_p/T_e has the opposite effect to that of increasing β. Similar qualitative conclusions can be drawn in the case of Ma's soliton; see figure 20.

Arguably, any qualitative conclusions drawn on the dependence of the rogue-like waveforms presented herein on physical parameters (β, temperature ratio T_e/T_p) can only be indicative. In particular, careful observation of the graphs of P and Q must be made before drawing conclusions about the physical effects of changing the relevant parameters, from figures 17–20. We see from the formulas (41)–(43) that the frequency of Akhmediev's (respectively, Ma's) breather depends on $\sqrt{Q/P}$ (respectively, Q), while the rate of decay

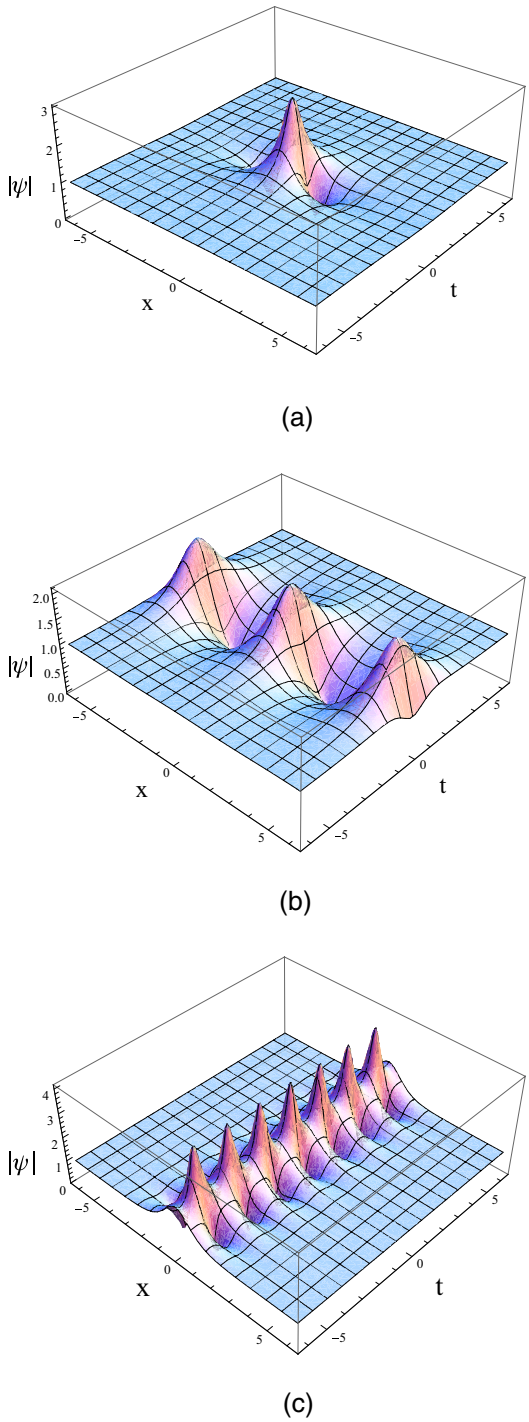

Figure 16. The three waveforms, as presented in the text, are here plotted against x and t: (*a*) Peregrine's 'Soliton', (*b*) Akhmediev's breather and (*c*) Ma's breather. The spatial and temporal behavior of each is clearly displayed. $P = Q = \varphi = 1$.

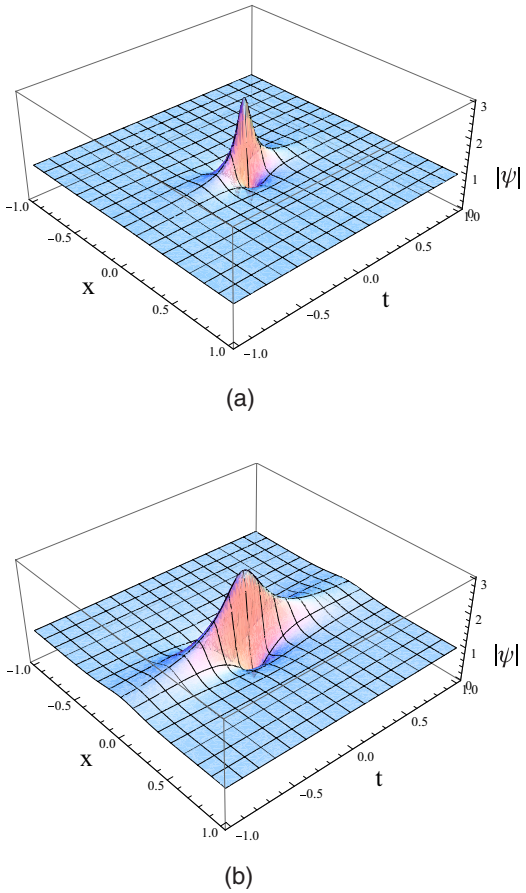

Figure 17. Peregrine's solution is depicted for two values of β. The first figure has $k = 2.5$, $T_p/T_e = 1$ and $\beta = 0$, whereas $\beta = 0.1$ in the second, which is of greater duration and spatial extension (i.e. less localized).

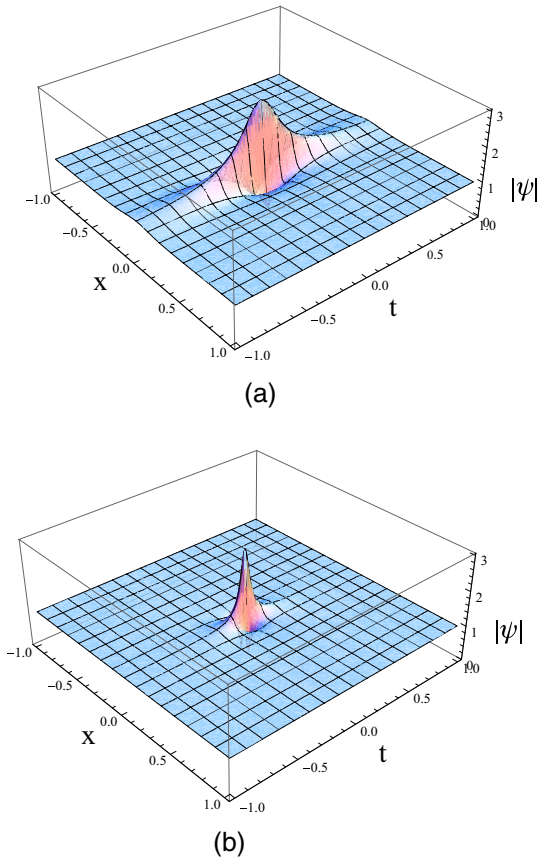

Figure 18. The duration in both space and time of Peregrine's solution is observed for two values of T_p/T_e. The first figure has $k = 3.5$, $T_p/T_e = 0.5$ and $\beta = 1$, whereas $T_p/T_e = 1.5$ in the second, which leads to a shorter duration.

of Peregrine's solution depends on both of these. Figures 3 and 4 show how the graph of Q is enlarged with β and with T_e/T_p, whereas P exhibits the opposite behavior. However, the rogue waves exist only in the regions where $PQ > 0$, so the position of the roots of P and Q are also important factors here. These same figures show how the roots are also shifted upwards. This combination of enlargement and translation might lead to an increase in the absolute value of Q (e.g. figure 3(*b*), $k = 0.55$, $\beta = 0, 0.1$). It might also decrease it (e.g. figure 3(*b*), $k = 0.65$, $\beta = 0, 0.1$) or leave it invariant (corresponding to the intersection of two graphs); see figure 21. In essence, whereas for one value of the carrier wavenumber k, the frequency of Ma's breather might increase with β, for another the effect might be the opposite. Therefore, the value of k chosen as a reference value in figures 17–20 also contributes to the qualitative profile of the waves.

10. Conclusions

We have investigated the nonlinear propagation of modulated electrostatic wavepackets propagating in an electron–positron–ion plasma. Electrons and positrons were assumed to follow a Fermi–Dirac distribution, while the ions are subject to a Fermi pressure. A fluid model was proposed and analyzed. Adopting a perturbative multiscale method, the evolution of the wave envelope was shown to be described by a nonlinear Schrödinger equation. Criteria for modulational instability were obtained, revealing a Benjamin–Feir type instability mechanism, and were formulated here in terms of the intrinsic plasma parameters.

The behavior of the wavepackets, as described by the NLSE (33), is determined by the values of the coefficients of the dispersive and the nonlinear terms, P and Q. The curves of P and Q both cross the k-axis. Naturally, there are very small intervals in k where either P or Q vanishes and wherein the evolution equation becomes respectively purely dispersive or nonlinear. If these regions are ignored (resorting to higher nonlinear or/and dispersive effects would be necessary in those small regions), then we have two classes of solution: the dark or gray solutions for $PQ < 0$, which are modulationally stable, and the bright solutions for $PQ > 0$, which can be unstable. Multiple-soliton interactions are possible in both cases.

The bright solutions comprise not only the familiar '*sech*' bell-shaped structures, but also periodic 'breather' type solutions, which represent highly localized oscillatory structures, and are thus good candidates for an analytical description of rogue waves. These include The Kuznetsov–Ma and Akhmediev's breather, and also, interestingly, Peregrine's 'soliton'. Rogue waves in dense plasmas are therefore *a priori* described by this model.

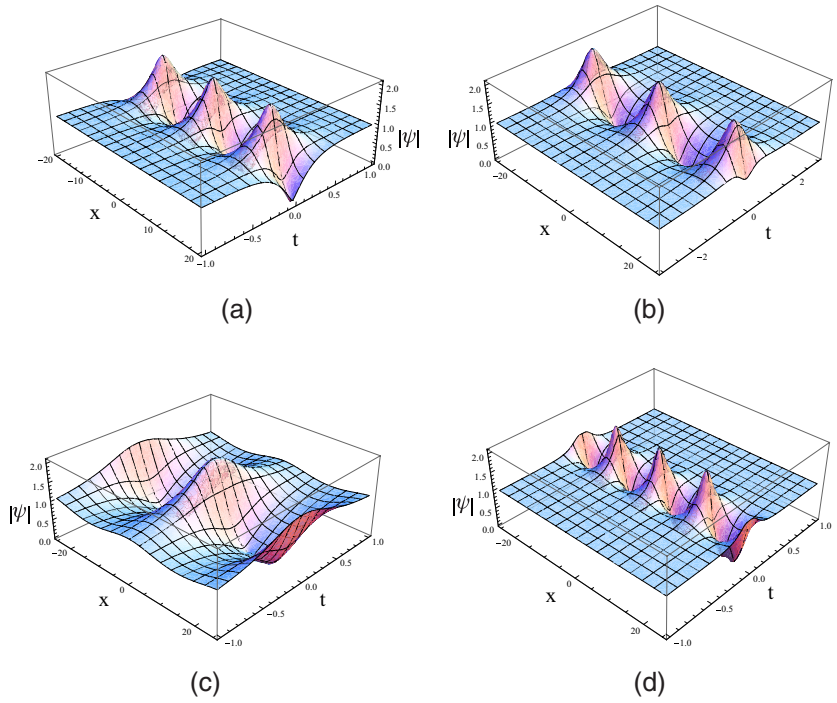

Figure 19. Plots of Akhmediev's breather for different values of β and T_e/T_p: (*a*), (*b*) $k = 2.5$, $T_p/T_e = 1$, $\beta = 0,\ 0.1$; (*c*), (*d*) $k = 3.5$, $\beta = 1$, $T_p/T_e = 0.5, 1.5$.

It may be added, for the sake of rigor, that the problem investigated (*quantum ion-acoustic* waves) is admittedly reminiscent of the propagation of (classical) ion-acoustic wavepackets (widely studied, both experimentally [54] and theoretically [16, 20, 40, 41, 55]) but nonetheless not physically amenable to that (and is clearly distinct in scope). While ion-acoustic waves are sustained by the electron thermal pressure, the key element here is the Fermi pressure of electrons and positrons, which is related to their density (assumed high, in dense plasmas). Certainly, the algebra (see the dimensionless system (9)–(11) above) is formally analogous to the classical one; importantly, however, all relevant coefficients depend on the physical properties of the quantum problem. In this respect, any comparison to the classical case would be of no real value beyond a formal, mathematically abstract level.

Our results are of relevance in ultradense situations where quantum effects are significant. In particular, we expect our findings to be important in the vicinity of compact stellar objects as well as in dense electron–positron–ion plasmas resulting from ultra-intense laser pulses [56].

Acknowledgments

MMK acknowledges financial support from Department of Employment and Learning Northern Ireland (DEL NI), in the form of a PhD studentship. IK acknowledges the UK Engineering and Physical Sciences Research Council (EPSRC) for support under grant No EP/I031766/1 (*'Fluid Theory and Simulation for Laser–Plasma Interactions'*). FH acknowledges financial support by CNPq (Conselho Nacional de Desenvolvimento Científico e Tecnológico), Brazil.

Appendix. Perturbative scheme: analytical expressions

The full solutions obtained up to second order in ϵ are given by the following expressions.

A.1. Analytical multi-harmonic solution(s) for the state variables

Electrostatic potential:

$$\phi \approx \epsilon\psi e^{i(kx-\omega t)} + \epsilon^2\left(\frac{C^0_{2_3}}{2}|\psi|^2 + C^2_{2_3}\psi^2 e^{2i(kx-\omega t)}\right) + \text{c.c.}$$

Ion density:

$$n \approx \frac{1}{2} + \epsilon\frac{c_1+k^2}{b}\psi e^{i(kx-\omega t)} + \epsilon^2\left(\frac{C^0_{2_1}}{2}|\psi|^2 + C^1_{2_1}\frac{\partial\psi}{\partial X_1}e^{i(kx-\omega t)} + C^2_{2_1}\psi^2 e^{2i(kx-\omega t)}\right) + \text{c.c.}$$

Ion-fluid speed:

$$v \approx \epsilon\frac{\omega}{k}\frac{c_1+k^2}{b}\psi e^{i(kx-\omega t)} + \epsilon^2\left(\frac{C^0_{2_2}}{2}|\psi|^2 + C^1_{2_2}\frac{\partial\psi}{\partial X_1} + C^2_{2_2}\psi^2 e^{2i(kx-\omega t)}\right) + \text{c.c.} \tag{A.1}$$

Expressions for various coefficients appearing in the harmonic amplitudes:

$$C^0_{2_1} = \frac{c_1\left(\frac{c_1+k^2}{b}\right)^2\left(2v_g\frac{\omega}{k} + g + \frac{\omega^2}{k^2}\right) - 2ac_2}{c_1 v_g^2 - ab - gc_1}, \tag{A.2}$$

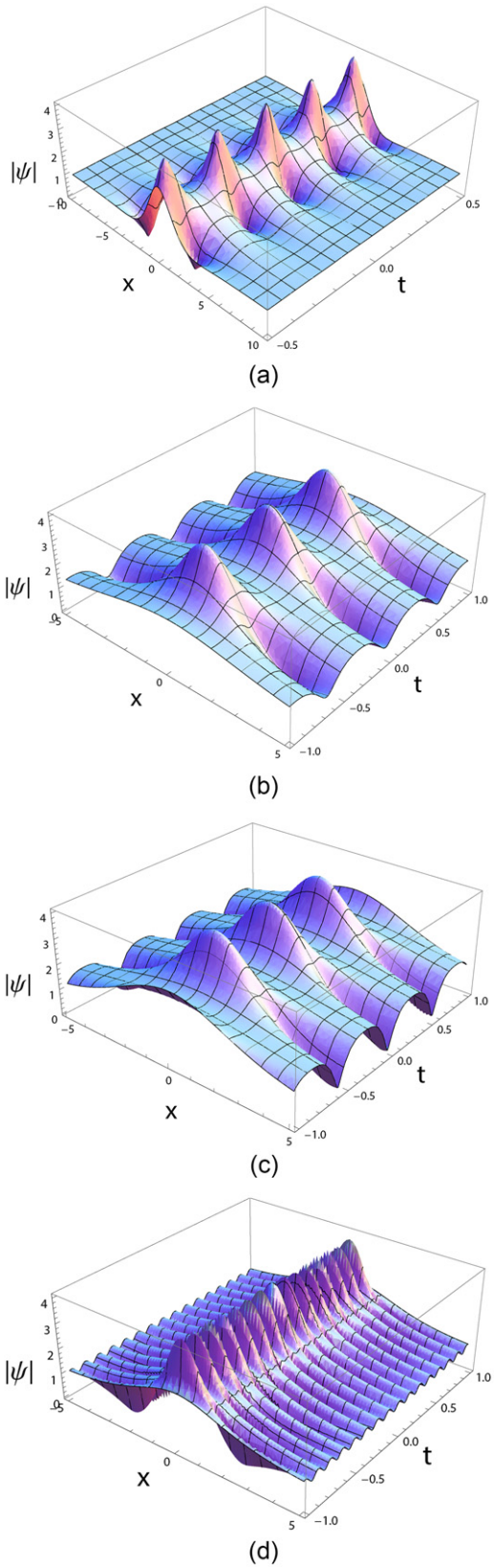

Figure 20. Plots of Ma's breather for different values of β and T_e/T_p: (*a*), (*b*) $k = 2.5$, $T_e/T_p = 1$, $\beta = 0, 0.1$; (*c*), (*d*) $k = 3.5$, $\beta = 1$, $T_p/T_e = 0.5,1.5$.

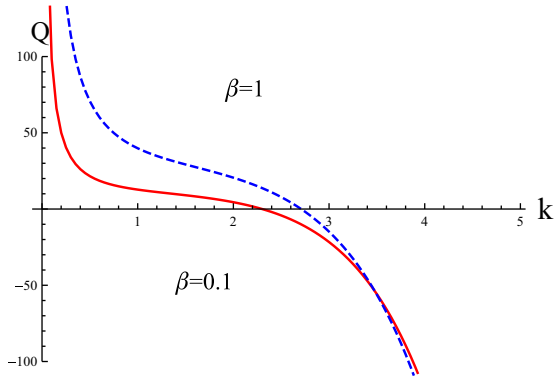

Figure 21. Depending on k, enlargement of the graph of Q, coupled with the translation of its root, can either increase, decrease or leave invariant $Q(k)$.

$$C^0_{2_2} = v_g C^0_{2_1} - 2\left(\frac{c_1 + k^2}{b}\right)^2 \frac{\omega}{k}, \tag{A.3}$$

$$C^0_{2_3} = \frac{b}{c_1} C^0_{2_1} - \frac{2c_2}{c_1}, \tag{A.4}$$

$$C^1_{2_1} = -\frac{2ik}{b}, \tag{A.5}$$

$$C^1_{2_2} = i\frac{c_1 + k^2}{b}\left(\frac{\omega}{k^2} - \frac{v_g}{k} - \frac{2\omega}{c_1 + k^2}\right), \tag{A.6}$$

$$C^2_{2_1} = \frac{c_1 + 4k^2}{b} C^2_{2_3} + \frac{c_2}{b}, \tag{A.7}$$

$$C^2_{2_2} = \frac{\omega}{k} C^2_{2_1} - \left(\frac{c_1 + k^2}{b}\right)^2 \frac{\omega}{k}, \tag{A.8}$$

$$C^2_{2_3} = \frac{\frac{(c_1+k^2)^2}{2b}(3\omega^2 + gk^2) - c_2(\omega^2 - gk^2)}{3k^2(\omega^2 - gk^2)}. \tag{A.9}$$

A.2. Coefficients in the NLSE (33)

$$P = \frac{v_g}{2k} - \frac{v_g^2}{2\omega} - \frac{2k}{c_1 + k^2}\left(v_g - g\frac{k}{\omega}\right), \tag{A.10}$$

$$Q = \frac{(\omega^2 - gk^2)(2c_2(C^0_{2_3} + C^2_{2_3}) + 3c_3)}{2\omega(c_1 + k^2)} - k(C^0_{2_2} + C^2_{2_2}) - \frac{(\omega^2 + gk^2)(C^0_{2_1} + C^2_{2_1})}{2\omega}. \tag{A.11}$$

A.3. Long-wave approximation

Below are given the expressions for the important functions for the domain, $k \ll 1$.

$$\frac{\omega^2}{k^2} = \frac{ab}{c_1 + k^2} + g \approx \frac{ab}{c_1} + g - \frac{ab}{c_1^2}k^2 = \eta_1^2 - \frac{ab}{c_1^2}k^2. \tag{A.12}$$

Defining $\eta_2 = \frac{ab}{2c_1^2\eta_1}$,

$$\omega \approx \eta_1 k - \eta_2 k^3, \tag{A.13}$$

$$v_g = \frac{\mathrm{d}\omega}{\mathrm{d}k} \approx \eta_1 - 3\eta_2 k^2, \tag{A.14}$$

$$\begin{aligned} \mathrm{C}^0_{2_1} &\approx \frac{c_1}{3ab}\left(2ac_2 - \frac{c_1^2}{b^2}\left(\frac{3ab}{c_1} + 4g\right)\right)\frac{1}{k^2}, \\ &\approx \frac{q_1}{k^2}, \end{aligned} \tag{A.15}$$

$$\mathrm{C}^0_{2_2} \approx v_g \mathrm{C}^0_{2_1} \approx \eta_1 \frac{q_1}{k^2}, \tag{A.16}$$

$$\mathrm{C}^0_{2_3} \approx \frac{b}{c_1}\mathrm{C}^0_{2_1} \approx \frac{b}{c_1}\frac{q_1}{k^2}, \tag{A.17}$$

$$\begin{aligned} \mathrm{C}^2_{2_3} &\approx \frac{\frac{c_1^2}{2b}(3ab + 4c_1 g) - abc_2}{3ab}\frac{1}{k^2} \\ &\approx \frac{m_3}{k^2}, \end{aligned} \tag{A.18}$$

$$\mathrm{C}^2_{2_1} \approx \frac{c_1}{b}\mathrm{C}^2_{2_3} \approx \frac{c_1 m_3}{bk^2}, \tag{A.19}$$

$$\mathrm{C}^2_{2_2} \approx \frac{\eta_1 c_1 m_3}{bk^2}. \tag{A.20}$$

Using these expressions, we obtain

$$P \approx -\frac{3ab}{2c_1^2\eta_1}k, \tag{A.21}$$

$$Q \approx \left(m_3 + \frac{b}{c_1}q_1\right)\frac{\gamma}{k}, \tag{A.22}$$

$$\gamma = \frac{abc_2}{c_1^2\eta_1} - \frac{\eta_1 c_1}{b} - \left(\frac{ab}{c_1} + 2g\right)\frac{c_1}{2\eta_1 b}. \tag{A.23}$$

References

[1] Haas F 2011 *Quantum Plasmas: An Hydrodynamic Approach* (New York: Springer)
[2] Eliasson B and Shukla P K 2008 *Phys. Scr.* **78** 025503
[3] Shukla P K and Eliasson B 2010 *Phys.—Usp.* **53** 51
[4] Manfredi G and Haas F 2001 *Phys. Rev.* B **64** 075316
[5] Gardner C L 1994 *SIAM J. Appl. Math.* **54** 409
[6] Ali S, Moslem W M, Shukla P K and Kourakis I 2007 *Phys. Lett.* A **366** 606
[7] Haas F 2003 *Phys. Plasmas* **10** 3858
[8] Khan S A and Mushtaq A 2007 *Phys. Plasmas* **14** 083703
[9] Khan S A, Mahmood S and Saleem H 2008 *Phys. Plasmas* **15** 082303
[10] Mushtaq A and Khan S A 2007 *Phys. Plasmas* **14** 052307
[11] Ali S, Moslem W M, Kourakis I and Shukla P K 2008 *New J. Phys.* **10** 023007
[12] Khan S A, Mahmood S and Ali S 2009 *Phys. Plasmas* **16** 044505
[13] Misra A P and Ghosh N K 2011 *Astrophys. Space Sci.* **331** 605
[14] Ghosh B, Chandra S and Paul S N 2011 *Phys. Plasmas* **18** 012106
[15] Taniuti T and Yajima N 1969 *J. Math. Phys.* **10** 1369
[16] Kourakis I and Shukla P K 2005 *Nonlinear Process. Geophys.* **12** 407
[17] Sulem P and Sulem C 1999 *Nonlinear Schrödinger Equation* (Berlin: Springer)
[18] Dauxois T and Peyrard M 2005 *Physics of Solitons* (Cambridge: Cambridge University Press)
[19] Daumont I, Dauxois T and Peyrard M 1997 *Nonlinearity* **10** 617–30
[20] Sultana S and Kourakis I 2011 *Plasma Phys. Control. Fusion.* **53** 045003
[21] Dysthe K, Krogstad H E and Müller P 2008 *Ann. Rev. Fluid Mech.* **40** 287
[22] Eliasson B and Shukla P K 2009 *J. Plasma Phys.* **76** 7
[23] Aoutou K, Tribeche M and Zerguini T H 2012 *Astrophys. Space Sci.* **340** 359
[24] Mehdipoor M and Esfandyari-Kalejah A 2012 *Astrophys. Space Sci.* **342** 93
[25] Rasheed A, Tsintsadze N L, Murtaza G and Chaudhary R 2011 *J. Plasma Phys.* **78** 133
[26] Dubinov A E, Kolotkov D Yu and Sazonkin M A 2012 *Tech. Math. Phys.* **57** 585
[27] Shukla P K, Kourakis I, Eliasson B, Marklund M and Stenflo L 2006 *Phys. Rev. Lett.* **97** 094501
[28] Grönlund A, Eliasson B and Marklund M 2009 *Europhys. Lett.* **86** 24001
[29] Lawton G 2001 *New Sci.* **170** 28
[30] Kharif C *et al* 2003 *Eur. J. Mech.* B **22** 603
[31] Akhmediev N, Ankiewicz A and Taki M 2009 *Phys. Lett.* A **373** 675
[32] Solli D R, Ropers C, Koonath P and Jalali B 2007 *Nature* **450** 1054
[33] Kibler B, Fatome J, Finot C, Millot G, Dias F, Genty G, Akhmediev N and Dudley J M 2010 *Nature Phys.* **6** 790
[34] Kibler B *et al* 2012 *Nature* **2** 463
[35] Ganshin A N, Efimov V B, Kolmakov G V, Mezhov-Deglin L P and McClintock P V E 2008 *Phys. Rev. Lett.* **101** 065303
[36] Chabchoub A, Hoffmann N P and Akhmediev N 2011 *Phys. Rev. Lett.* **106** 204502
[37] Stenflo L and Marklund M 2010 *J. Plasma Phys.* **76** 293
[38] Yan Z-Y 2010 *Commun. Theor. Phys.* **54** 947
[39] Ivancevic V G 2010 *Cogn. Comput.* **2** 17
[40] Kako M 1974 *Prog. Theor. Phys. Suppl.* **55** 120
[41] Kakutani T and Sugimoto N 1974 *Phys. Fluids* **17** 1617
[42] Dubinov A E and Sazonkin M A 2010 *J. Exp. Theor. Phys.* **111** 865
[43] Abramowitz M and Stegun I 1965 *Handbook of Mathematical Functions* (New York: Courier Dover)
[44] Fortov V 2009 *Phys.—Usp.* **6** 615
[45] Zakharov V E and Shabat A B 1973 *Sov. Phys.—JETP* **37** 23
[46] Drazin P G and Johnson R S 1989 *Solitons: An Introduction* (Cambridge: Cambridge University Press)
[47] Fedele R, Schamel H and Shukla P K 2002 *Phys. Scr.* **T98** 18
Fedele R and Schamel H 2002 *Eur. Phys. J.* B **27** 313
[48] Akhmediev N, Soto-Crespo J M and Ankiewicz A 2009 *Phys. Lett.* A **373** 2137
[49] Peregrine D H 1983 *J. Aust. Math. Soc.* B **25** 16
[50] Dysthe K and Trulsen K 1999 *Phys. Scr.* **T82** 48
[51] Ruderman M S 2010 *Eur. Phys. J.-ST* **185** 57
Moslem W M *et al* 2011 *Phys. Rev.* E **84** 066402
[52] Veldes G, Borhanian J, McKerr M, Saxena V, Frantzeskakis D J and Kourakis I 2013 *J. Opt.* **15** 064003
[53] Bailung H, Sharma S K and Nakamura Y 2011 *Phys. Rev. Lett.* **107** 255005
[54] Ikezi H, Schwarzenegger K, Simons A L, Ohsawa Y and Kamimura T 1978 *Phys. Fluids* **21** 239
[55] Kourakis I and Shukla P K 2003 *Phys. Plasmas* **10** 3459
Kourakis I and Shukla P K 2004 *Eur. Phys. J.* D **28** 109
[56] Kuznetsova I and Rafelski J 2012 *Phys. Rev.* D **85** 085014